Research Paper

First-in-human study of PET and optical dual-modality image-guided surgery in glioblastoma using ^{68}Ga-IRDye800CW-BBN

Deling Li[1,3,4]*, Jingjing Zhang[2]*, Chongwei Chi[3]*, Xiong Xiao[1,4], Junmei Wang[5], Lixin Lang[6], Iqbal Ali[6], Gang Niu[6], Liwei Zhang[1,4], Jie Tian[3✉], Nan Ji [1,4✉], Zhaohui Zhu[2✉], Xiaoyuan Chen[6✉]

1. Department of Neurosurgery, Beijing Tiantan Hospital, Capital Medical University, Beijing, China
2. Department of Nuclear Medicine, Peking Union Medical College Hospital, Chinese Academy of Medical Sciences and Peking Union Medical College, Beijing, China
3. Key Laboratory of Molecular Imaging, Chinese Academy of Science, Beijing, China
4. China National Clinical Research Center for Neurological Diseases (NCRC-ND), Beijing, China
5. Department of Neuropathology, Beijing Neurosurgical Institute, Capital Medical University, Beijing, China
6. Laboratory of Molecular Imaging and Nanomedicine (LOMIN), National Institute of Biomedical Imaging and Bioengineering (NIBIB), National Institutes of Health (NIH), Bethesda, Maryland, United States

*These authors contributed equally to this work.

✉ Corresponding authors: Email: Jie Tian, jie.tian@ia.ac.cn; Nan Ji, cnpsycho@163.com; Zhaohui Zhu, zhuzhh@pumch.cn; Xiaoyuan Chen, shawn.chen@nih.gov.

Abstract

Purpose: Despite the use of fluorescence-guided surgery (FGS), maximum safe resection of glioblastoma multiforme (GBM) remains a major challenge. It has restricted surgeons between preoperative diagnosis and intraoperative treatment. Currently, an integrated approach combining preoperative assessment with intraoperative guidance would be a significant step in this direction.

Experimental design: We developed a novel ^{68}Ga-IRDye800CW-BBN PET/near-infrared fluorescence (NIRF) dual-modality imaging probe targeting gastrin-releasing peptide receptor (GRPR) in GBM. The preclinical *in vivo* tumor imaging and FGS were first evaluated using an orthotopic U87MG glioma xenograft model. Subsequently, the first-in-human prospective cohort study (NCT 02910804) of GBM patients were conducted with preoperative PET assessment and intraoperative FGS.

Results: The orthotopic tumors in mice could be precisely resected using the near-infrared intraoperative system. Translational cohort research in 14 GBM patients demonstrated an excellent correlation between preoperative positive PET uptake and intraoperative NIRF signal. The tumor fluorescence signals were significantly higher than those from adjacent brain tissue *in vivo* and *ex vivo* (p < 0.0001). Compared with pathology, the sensitivity and specificity of fluorescence using 42 loci of fluorescence-guided sampling were 93.9% (95% CI 79.8%-99.3%) and 100% (95% CI 66.4%-100%), respectively. The tracer was safe and the extent of resection was satisfactory without newly developed neurologic deficits. Progression-free survival (PFS) at 6 months was 80% and two newly diagnosed patients achieved long PFS.

Conclusions: This initial study has demonstrated that the novel dual-modality imaging technique is feasible for integrated pre- and intraoperative targeted imaging *via* the same molecular receptor and improved intraoperative GBM visualization and maximum safe resection.

Key words: glioblastoma; dual-modality imaging; positron emission tomography (PET); near-infrared fluorescence; intraoperative imaging; gastrin-releasing peptide receptor

Introduction

Maximum safe resection of magnetic resonance (MR) contrast-enhanced tumor is the current goal for the treatment of both newly-diagnosed [1] and recurrent [2] glioblastoma multiforme (GBM). It is extremely challenging to achieve this goal because of the aggressive and infiltrative growth, especially for GBM involving eloquent areas in the brain. Preoperative imaging assessment and intraoperative image-guided surgery are key for this aim.

Several trials confirmed that even in recurrent GBM patients, complete or maximum resection of enhancing part could be beneficial [2]. However, for recurrent GBM following surgery, radiotherapy, and chemotherapy, preoperative contrast-enhanced MRI alone cannot differentiate recurrence from radionecrosis. In this respect, positron emission tomography (PET) and MR spectroscopy (MRS) imaging have some added value [3]. Also, for newly-diagnosed GBM, biological tumor volume determined by ^{18}F-fluoroethyl-L-tyrosine (FET) PET imaging was an important prognostic biomarker and assisted in maximal PET-guided tumor resection [4].

Intraoperatively, the tumor margins are indistinguishable from the normal brain using a white-light microscope. Fluorescence-guided surgery (FGS) by 5-aminolevulinic acid (5-ALA) permits real-time intraoperative guidance for tumor visualization and benefits patient survival [5-13]. However, 5-ALA cannot be evaluated preoperatively for overall uptake, especially for the secondary GBM which might have lower grade tumor regions with low sensitivity to this agent [14]. Another clinically used optical probe, fluorescein sodium, is a nonspecific fluorophore that is extracellular and associated with breakdown of the BBB. At present, techniques for preoperative evaluation by PET and MRI and intraoperative image-guided surgery using the same molecular target in glioma patients are not available.

We hypothesized that intraoperative optical imaging of the tumor-specific molecular target positively labeled by preoperative PET would be of significant advantage for GBM surgery navigation. One of the molecular targets in GBM is the gastrin-releasing peptide receptor (GRPR), which has been shown to be overexpressed and play a role in the development of gliomas [15]. We previously developed ^{68}Ga-labeled bombesin (BBN) peptide derivative NOTA-Aca-BBN (7-14) (denoted as ^{68}Ga-BBN), which specifically targets GRPR in gliomas with a high tumor-to-background ratio [16]. In this study, we extended this concept by conjugating IRDye800CW, a near-infrared fluorophore [17-24], to form the ^{68}Ga-IRDye800CW-BBN PET/NIRF dual-modality imaging tracer (**Fig. 1A**). We assessed our hypothesis

in a preclinical model and defined the optimal criteria for translation to the first-in-human study. We analyzed the accuracy of this technique for tumor detection by correlating intraoperative NIRF signal with the pathology of image-guided sampling and its effectiveness for improving the extent of resection of both newly diagnosed and recurrent GBM. Furthermore, we evaluated the safety and adverse effects of optical probe utilization.

Materials and Methods

Study design

A novel PET/NIRF dual-modality imaging probe, ^{68}Ga-IRDye800CW-BBN, was evaluated for its accuracy and safety in a preclinical orthotopic U87MG glioma xenograft model and in a small cohort of GBM patients. Patients with MRI imaging and/or pathological evidence of newly diagnosed or recurrent GBM were enrolled with a written informed consent during the period of April 2016 to October 2017 in Peking Union Medical College hospital and Beijing Tiantan Hospital. Exclusion criteria were mental illness; severe liver or kidney disease with serum creatinine > 3.0 mg/dl; any hepatic enzyme level 5 times or more than normal upper limit; severe allergy or hypersensitivity to IV radiographic contrast; claustrophobia to accept the PET/CT or PET/MRI scanning; pregnancy or breast feeding. The aim of this study was to explore the feasibility of the dual-modality imaging tracer and intraoperative NIRF navigation system for the surgical resection of gliomas while avoiding severe neurological deficits. We, therefore, did not strictly exclude the tumor location, such as the tumors adjacent to or even involving basal ganglia, thalamus or other eloquent areas. The surgeons were blinded to the neuropathology and the neuro-radiologists and neuropathologists were blinded to intraoperative fluorescence. The trial was registered at ClinicalTrial.Com (NCT 02910804).

Molecular imaging probe synthesis

Waters 600 high-performance liquid chromatography (HPLC) system with a Waters 996 Photodiode Array Detector (PDA) using a preparative C_{18} HPLC column (PROTO 300 C_{18} 5 µm, 250 x 20 mm, Higgins Analytical, Inc.) was used for peptide purification. The peptides were analyzed using a Perkin-Elmer 200 series HPLC pump with a Waters 2487 UV detector and an analytical C_{18} HPLC column (Waters Symmetry C_{18} 5 µm, 150 x 3.9 mm). Mass spectra were obtained with a Waters LC-MS system (Waters, Milford, MA) that included an Acquity UPLC system coupled to a Waters Q-Tof Premier high-resolution mass spectrometer. All chemicals were purchased from Sigma-Aldrich (St. Louis, MO) unless otherwise

stated in the procedure.

Preparation of NOTA-IRDye800CW-BBN

To a 20 mL glass vial containing 27.5 mg of BBN (7-14) in 2.6 mL of DMF 9.5 mg of Fmoc-lys(Boc)-OH, 25 µL of N,N-diisopropylethylamine (DIPEA) and 5 µL of diethyl cyanophosphonate (DECP) were added. The mixture was stirred at room temperature for 2 h and analyzed with LC-MS that showed formation of desired product Fmoc-lys(Boc)-BBN. Fmoc protecting group was removed by adding 0.6 mL of piperidine and stirred at room temperature for 1 h. HPLC purification and freeze-drying gave 18.5 mg lys(Boc)-BBN with 71% yield. LC-MS: $[MH]^+$ = 1279.5933 (m/z), calc: 1280.7063 ($C_{60}H_{96}N_{16}O_{13}S$).

Lys(Boc)-BBN (18.5 mg) was dissolved in 2 mL of DMSO, DIPEA (20 µL) and 2,2'-(7-(2-((2,5-dioxopyrrolidin-1-yl)oxy)-2-oxoethyl)-1,4,7-triazonane-1,4-diyl)diacetic acid (NOTA-NHS ester, Che-Matech) (24.0 mg, 2 eq.) were added to the solution. The mixture was stirred at room temperature for 20 min and monitored with HPLC. After lys(Boc)-BBN was consumed and LC-MS showed desired product NOTA-lys(Boc)-BBN, DMSO was removed by freeze drying and Boc protecting group was removed by 0.1 mL TFA. The mixture was then purified with HPLC to give 6.5 mg NOTA-lys-BBN with (or at) 30.6% yield.

LC-MS: $[MH]^+$ = 1464.6552 (m/z), calc: 1465.7864 ($C_{67}H_{107}N_{19}O_{16}S$).

To a 20 mL glass vial containing 6.5 mg NOTA-lys-BBN in 1 mL of DMSO 6.0 mg of IRdye800CW NHS ester (LI-COR, Lincoln, Nebraska) and 10 µL DIPEA were added. The mixture was stirred at room temperature for 1 h and purified with HPLC to give 2 mg of the desired product with 18.5% yield and >97% purity. LC-MS: $[(MHH)/2]^{++}$ = 1224.9103 (m/z), calc: 2450.0165 ($C_{113}H_{159}N_{21}O_{30}S_5$).

GBM model preclinical research

All animal experiments were approved by the Institutional Animal Care and Use Committee of Peking University. Five-week-old athymic female BALB/c nude mice, purchased from the Department of Experimental Animals, Peking University Health Science Center, were orthotopically transplanted with 1×10^6 U87MG cells in PBS into the brain. After 2 weeks, the mice were anesthetized with an injection of a mixture of ketamine, xylene, and sterile distilled water (0.2 mL) at a ratio of 7:3:4. Based on the results of the feasibility study, image-guided surgery was performed on a small animal operating table (Py2-501213, Harvard, USA) using our surgical navigation system for precise tumor detection after intravenous injection of 0.1 mg (0.1 mL) of IRDye800CW-BBN probe.
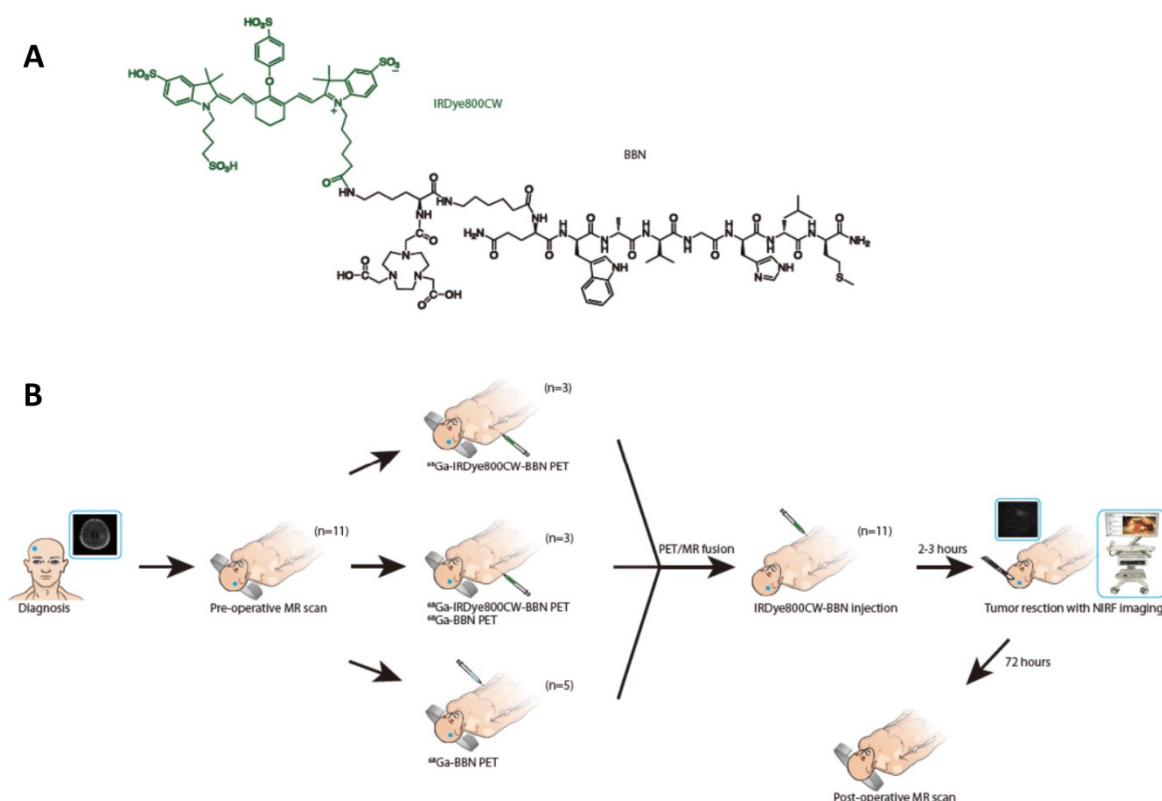
Fig. 1. The chemical structure of IRDye800CW-BBN tracer and the scheme of this first-in-human study. **(A)** Chemical structure of IRDye800CW (green) with the BBN (black). **(B)** Enrollment and research scheme for the GBM patients.

A total of 18 mice were placed under our imaging system. Three experienced surgeons removed the orthotopic tumor under NIR fluorescence guidance. All fluorescent tumor tissues were excised during surgery and frozen at -80 °C in optimum cutting temperature (OCT) compound (Leica, Germany) immediately after surgery. The tumors were cryosectioned (Leica CM1950, Leica) to yield sections of 4-µm thickness for hematoxylin and eosin (H&E) staining. The frozen OCT sections were fixed in acetone for 10 min.

PET imaging and image analysis

^{68}Ga-BBN was synthesized following a procedure reported previously [16, 25]. IRDye800CW-BBN was synthesized under current good manufacturing practices (cGMP) by LI-COR company [25]. The radiolabeling of ^{68}Ga-IRDye800CW-BBN was performed in a sterile hot cell. ^{68}Ga was eluted from a ^{68}Ge/^{68}Ga generator (Eckert &Ziegler, Berlin, Germany) using 0.05 M HCl and mixed with 1.25 M NaOAc buffer to adjust the pH value to 4.0. The mixture was then directly transferred to a 1 mL plastic tube containing 40 µg of NOTA-IRDye800CW-BBN. After shaking, the mixture was incubated in a heating block at 100 °C for 10 min. Then the reaction mixture was cooled down, dissolved in sterile phosphate-buffered saline, and passed through 0.22 µm aseptic filtration membrane. Thin-layer liquid chromatography (BIOSCAN, USA) was used to test the radiochemical purity with CH3OH:NH4OAc (v/v 1:1) as the developing solution. The radiochemical purity of the product ^{68}Ga-IRDye800-BBN was over 95%.

Among the 14 patients, 4 patients received simultaneous PET/MR and the other 10 patients received PET/CT. ^{68}Ga-BBN PET/CT and ^{68}Ga-BBN PET/MR scanning was performed at 30 min after tracer administration. ^{68}Ga-IRDye800CW-BBN PET/CT and ^{68}Ga-IRDye800CW-BBN PET/MRI was performed at 30 min and 60 min after tracer administration. A single dose of 74-148 MBq ^{68}Ga-BBN or ^{68}Ga-IRDye800CW-BBN (1.85 MBq per kilogram of body weight) was injected intravenously. Brain PET was performed with 10-min PET acquisition covering the whole head of the patient. The images were transferred to a MMWP workstation (Siemens) for analysis.

For the 10 patients who underwent ^{68}Ga-BBN and/or ^{68}Ga-IRDye800CW-BBN PET/CT, PET images were co-registered to MR images with automatic image registration and manual positioning was performed as needed.

General biodistribution and temporal and intersubject stability were determined by visual analysis. Volumes of interest for normal brain tissues and the concerned lesions were drawn using 3-dimensional ellipsoid isocontouring, and the radioactivity concentrations and SUVs in these volumes of interest were obtained using the workstation software. The results were expressed as SUV_{mean} and SUV_{max}. MR and PET images were compared and then fused together to visualize the uptake area and the adjustment of the boundaries.

Clinical assessment and follow up

Before each time of tracer injection for preoperative PET imaging or intraoperative FGS, we obtained a 12-lead electrocardiogram (ECG) for patients, and the vital signs including blood pressure, heart rate, respiratory rate and blood oxygenation were monitored. Any discomforts were simultaneously recorded, such as nausea, vomiting, short breath, *etc*. The baseline parameters in blood (complete chemistries, complete metabolic panel and erythrocyte, white cell or platelet count) were obtained. For safety assessment, the same blood tests were repeatedly performed within 3 days after tracer usage. To rule out the pyrogenic effect, the patient temperature was recorded twice daily. If the temperature was over 38.5 °C, the number of postoperative day was recorded and the suspected reason for fever was assessed, including postoperative central nervous system infection (PCNSI), aseptic meningitis, pneumonia, urinary tract infection, *etc*. Cerebrospinal fluid analysis *via* lumber puncture was necessary for fever differential diagnosis. For assessing patients' neurologic deficits or neuropsychological effect correlating to tumor resection, preoperative symptoms and neurologic examination were recorded and newly developed postoperative neurologic deficits were recorded on the postoperative day one (POD1) and POD7. The patient survival was followed up by enhancing MRI every three months. The tumor progression and overall survival were based on RANO criteria [26]. The PFS-6 was defined as the proportion of patients with no progression 6 months after operation.

Intraoperative NIRF imaging

1.0 mg IRDye800CW-BBN of 1 mL saline was injected intravenously 2 h before anesthesia induction. FGS was performed using our intraoperative imaging system, as previously described [27-30]. Near-infrared (NIR) fluorescence images were acquired and displayed in real time. Based on our previous methods, we further updated our system to provide an improved optical path design, optimized handheld light source, and efficient image algorithms for best visualization. Relative fluorescent units (RFU) were measured for tumor and background, and

signal-to-background ratio (SBR) was calculated by dividing *in vivo* tumor or *ex vivo* tissue RFU by respective RFU [18, 31].

If the tumor involved the cortex area, the handheld NIRF detector was used immediately after dura opening to visualize whether the positive fluorescence was obvious and determine the tumor borderline. The tumor was resected along the boundary (usually within the region of reactive gliosis) to decrease blood loss under the guidance of white-light microscope (M205FA, Leica, Germany). The tumor bed or cavity was then illuminated with NIRF detector. If fluorescence was present in safe area (likely not the direction of eloquent area), the tissue was further resected and the specimens from different loci were separately submitted to neuropathology. If safe, one biopsy form nonfluorescent area around tumor cavity was collected. However, for the patients with tumors involving eloquent areas, no obligatory tissue biopsy from nonfluorescent area was obtained. The RFU of *ex vivo* tissues were also measured.

These patients did not receive any other fluorescence-guided operation intraoperatively. Any other techniques, such as intraoperative ultrasound and MRI, were not utilized. If a navigation system was used, the simultaneous PET/MR was directly imported in the platform of Medtronic Navigation system STEALTHSTATION TREON Plus (No.108 8309). If only PET/CT was performed, the enhanced MRI imaging and ^{68}Ga-BBN or ^{68}Ga-IRDye800CW-BBN PET/CT imaging were imported and fused in the same platform. The navigation system was only used for incision, bone flap, cortex incision region or cortical fistulization design and was not used while resecting the tumor or dissecting the residual tumor around the tumor cavity.

Image analysis

The preoperative contrast-enhanced MRI was performed within 1 week preoperatively. Early postoperative MRI was obtained within 72 h after operation. All MR scans were performed on a 3.0 T scanner with a head coil, and 0.1 mmol/kg body weight Magnevist was injected intravenously. Slice thickness was 5 mm. All MRI scans were evaluated centrally at the department of neuroradiology in Beijing Tiantan Hospital.

The volumes were calculated with manual segmentation of tumor outline using Picture Archiving and Communication Systems (PACS) system (Neusoft PACS Version 5.5) and the areas on each slice were added and the sum was multiplied by the thickness of each section [32]. The contrast-enhanced volume was defined as the area of high signal intensity on contrast-enhanced T_1-weighted (T1W)

MRI.

The completeness of tumor resection was determined based on the contrast-enhanced volume less than 0.175 cm^3 [5]. The extent of resection was calculated as (preoperative contrast- enhanced volume-postoperative contrast enhanced volume)/ preoperative contrast enhanced volume *100%.

Pathological analysis

The samples were managed according to the protocol published previously [16]. The pathology was determined by three neuropathologists separately, and if any discrepancy, the consensus was reached by another higher-level pathologist. The criteria of pathology diagnosis are the 2016 World Health Organization Classification of Tumors of the Central Nervous System (CNS WHO) [33].

Statistical analysis

Statistical analysis was performed by using GraphPad Prism 6.0. Values were expressed as means ± SD. The sensitivity, specificity and other diagnostic parameters were defined [34]. The RFU and SBR were compared by using the Paired t test.

Results

Preclinical optical imaging of GBM animal model

We examined whether our probe could delineate clear margins of orthotopic brain tumors *in situ* and further refine tumor resection. As shown in **Fig. 2**, initial post-injection images revealed not only the bulk tumor but also highlighted the invasive and irregular tumor margins.

During the traditional surgery of the orthotopic tumors, the remnant tumor tissues could not be detected by the naked eye even by three experienced surgeons and it was difficult to avoid the dissection of healthy brain tissues. For mice experiment, we injected the IRDye800CW-BBN probe, orthotopic tumors could be completely resected using the near-infrared intraoperative system. During the entire operation, the orthotopic brain tumor margins were clearly visualized assisting the surgeons to perform the precise resection of tumors. If the fluorescence signal indicated the presence of remnant tumor tissues around the margins of the surgical cavity, additional surgery of the tumor margins could be performed and confirmed by pathology.

Overall characteristics of this cohort

Fourteen patients were enrolled in this cohort. There were 12 males and 2 females, and the median age was 47 years old. There were 8 newly diagnosed and 6 recurrent GBM. Among the 6 recurrent GBM

patients, two patients had the first diagnosis of glioblastoma multiforme, while the other 4 had anaplastic astrocytoma. According to the classification by Sawaya and colleagues [35], 10 patients presented with grade III lesions (tumors in eloquent brain areas), 2 patients with grade II (near-eloquent brain areas) and 2 patients with grade I lesions. Median preoperative tumor volume was 55.49 cm^3 (range, 7.00-159.19 cm^3) based on contrast-enhanced T1W MRI.

Preoperative PET imaging and biodistribution

The biodistribution of radiotracer ^{68}Ga-BBN in healthy volunteers and glioma patients have previously been reported [16]. All 14 patients underwent preoperative PET. Three of the patients accepted PET scanning with both ^{68}Ga-BBN and ^{68}Ga-IRDye800CW-BBN within one week for comparative analysis of the two tracers. We observed similar biodistribution in normal brain tissues with the standardized uptake value SUV$_{mean}$ of 0.10 ± 0.02. ^{68}Ga-BBN PET showed prominent tracer accumulation in the lesions. Quantitative analysis yielded SUV$_{max}$ and SUV$_{mean}$ values of 1.70 ± 0.39 and 1.08 ± 0.30, respectively, and tumor-to-background (T/B) ratios based on SUV$_{max}$ and SUV$_{mean}$ were 19.54 ± 4.20 and 12.12 ± 2.38, respectively. In ^{68}Ga-IRDye800CW-BBN PET, additional uptake of brain blood pool was observed at 30 and 60 min after injection, as well as a low background signal in the normal brain tissues with the SUV$_{mean}$ of 0.08 ± 0.03. Similar tracer accumulation within the brain lesions was detected on ^{68}Ga-IRDye800CW-BBN PET scans compared with ^{68}Ga-BBN for the same patients (**Fig. 3**). Quantitative analysis yielded SUV$_{max}$ and SUV$_{mean}$ values on ^{68}Ga-IRDye800CW-BBN PET of 1.47 ± 0.26 and 1.01 ± 0.22, respectively, and T/B ratios based on SUV$_{max}$ and SUV$_{mean}$ were 19.61 ± 2.76 and 13.43 ± 1.27, respectively. Thus, no significant difference of radiotracer biodistribution in normal brain tissues and tumor lesions was found between ^{68}Ga-BBN and ^{68}Ga-IRDye800CW-BBN PET ($P > 0.05$).

The remaining 11 patients underwent ^{68}Ga-BBN PET (n = 7) or ^{68}Ga-IRDye800CW-BBN PET (n = 4). ^{68}Ga-BBN PET imaging showed positive results in 7 patients (4 newly diagnosed and 3 recurrent) with quantitative SUV$_{max}$ values of 1.67 ± 0.39 and T/B ratios of 18.09 ± 3.5. ^{68}Ga-IRDye800CW-BBN PET showed tracer accumulation in the 4 patients (2 newly diagnosed and 2 recurrent) with quantitative SUV$_{max}$ and T/B ratios of 1.01 ± 0.39 and 14.5 ± 4.3, 0.93 ± 0.25 and 20.0 ± 2.5 at 30 min and 60 min, respectively.
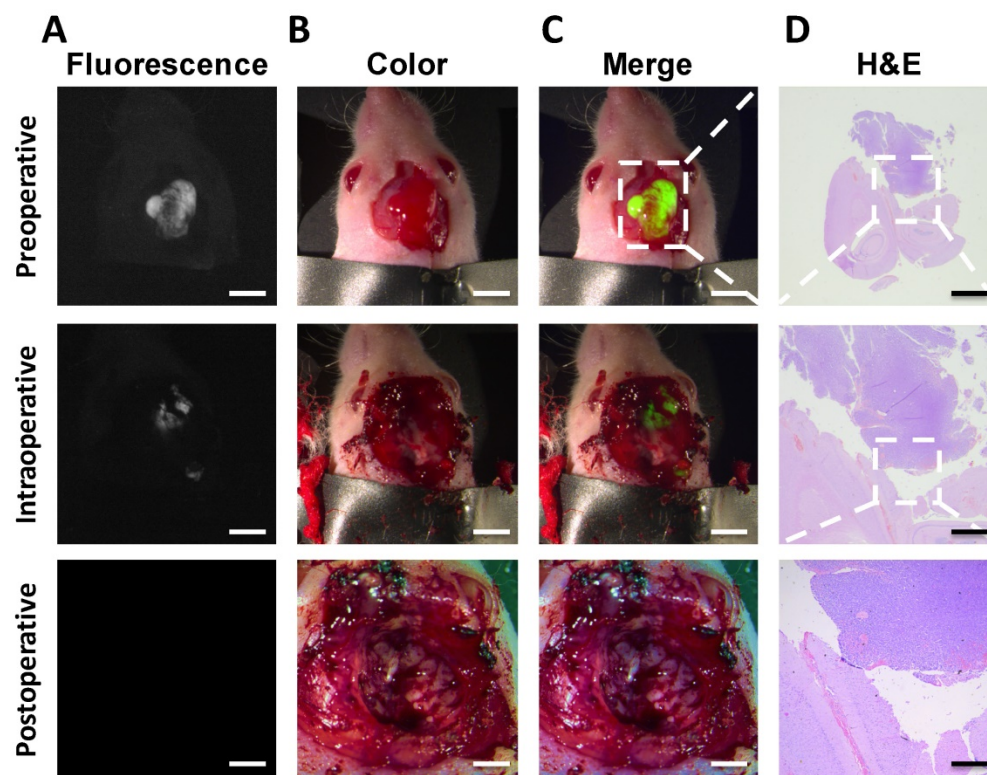
Fig. 2. The intraoperative fluorescence-guided surgery of GBM. The fluorescence image confirmed tumor existence of the nude mice **(A)**. color images were acquired to evaluate the residuals in a step-by-step manner **(B)**. The fluorescence and color images showed that all the fluorescent tissues were removed from the mouse **(C)**. The H&E images confirmed the results of tumor **(D)**. Scale bars, preoperative row, 5 mm; intraoperative row, 5 mm; postoperative row, 3 mm. Scale bar, H&E column 2, 1, 0.2 mm, respectively for rows 1-3.

Intraoperative optical and postoperative imaging assessment

Among the 14 patients enrolled, tumors from 12 patients were in the cortex and white matter areas, whereas the other two were deeply seated in the thalamus and medial temporal and insula (Patients 4 and 5 in **Table 1**). In the case of 12 patients, the fluorescence was illuminated immediately after opening the dura. The boundary of normal cortex and the tumor could be readily outlined. However, in Patients 4 and 5 with deep-seated tumors, after initial cortical fistulization, the brain retractor was utilized for sufficient tumor exposure. In these two cases, the fluorescence signal was weaker (**Fig. S1B**) than in patients with tumors involving the cortex area and those who had a much larger cavity after surgical tumor debulking.

Table 1, Clinical characteristics, tumor location, clinical symptoms and fluorescence-guided surgery of this GBM cohort. The quantitative assessment of preoperative tumor volume in MRI and PET, extent of resection as well as the intraoperative fluorescence was recorded.

Patient No.	Gender (M/F)	Age	Tumor Location	Eloquence Grade	Recurrent tumor (Y/N)	Preoperative T1 post-Gd enhancement (cm³)	Postoperative T1 post-Gd enhancement (cm³)	% of resection	Complete resection (Y/N, <175 mm³)	Visible fluorescence after resection (Y/N)	Fluorescence density & location (same with postoperative MRI enhancement? Y/N)	Preoperative symptoms	Postoperative status
1	M	48	Right Parietal/ Occipital	III	N	83.09	0.108	99.9	Y	Y	Minimal, deep cavity (Y)	Right-sided hemiparesis (IV)	Same
2	M	59	Left Parietal/ Occipital	III	N	16.90	0.145	99.1	Y	N	/	Intracranial hypertension; facial numbness	Right-sided hemiparesis (II), recovered 1 month postoperatively
3	M	55	Left Frontal/ Temporal /Parietal	III	N	71.57	0	100	Y	N	/	Right extreme numbness; fine motor control difficulty	Same
4	M	15	Thalamus / Midbrain	III	N	14.53	0.510	96.5	N	Y	Deep cavity (Y)	Intracranial hypertension; left vision difficulty; hearing loss	Improved
5	M	46	Left Temporal / Insula	II	N	8.51	0.800	90.6	N	Y	Deep cavity (Y)	Intracranial hypertension; Right-sided hemiparesis (II)	Improved
6	M	37	Left Frontal & Insula	III	N	29.67	0	100	Y	N	/	Intracranial hypertension	Improved
7	M	64	Left Temporal & Insula	III	N	87.76	0.152	98.3	Y	N	/	Intracranial hypertension; dysphonia	Improved
8	M	53	Right Temporal	I	N	7.00	0	100	Y	N	/	Secondary epilepsy	Improved
9	F	49	Left Frontal/ Parietal/Insula	III	Y	96.20	7.30	92.4	N	Y	Anterior cavity (Y)	Right-sided hemiparesis (III-IV); motor aphasia	Same
10	M	60	Right Frontal	I	Y	57.68	0.158	99.7	Y	N	/	Epilepsy	Improved
11	F	39	Right Frontal/ corpus callusum	III	Y	53.31	8.460	84.1	N	Y	Deep cavity & corpus callosum (Y)	Intracranial hypertension	Improved
12	M	31	Left Frontal	II	Y	24.55	1.793	92.7	N	Y	Deep cavity (Y)	Intracranial hypertension	Improved
13	M	28	Right Frontal/ Temporal	III	Y	57.86	14.649	74.7	N	Y	Anterior cavity (Y)	left-sided hemiparesis (I-II)	Same
14	M	42	Left Temporal / Occipital	III	Y	195.19	3.413	98.3	N	Y	Anterior cavity & splenium of corpus callosum (Y)	Headache; hemianopia; writing inability; memory deficiency	Headache; memory improved
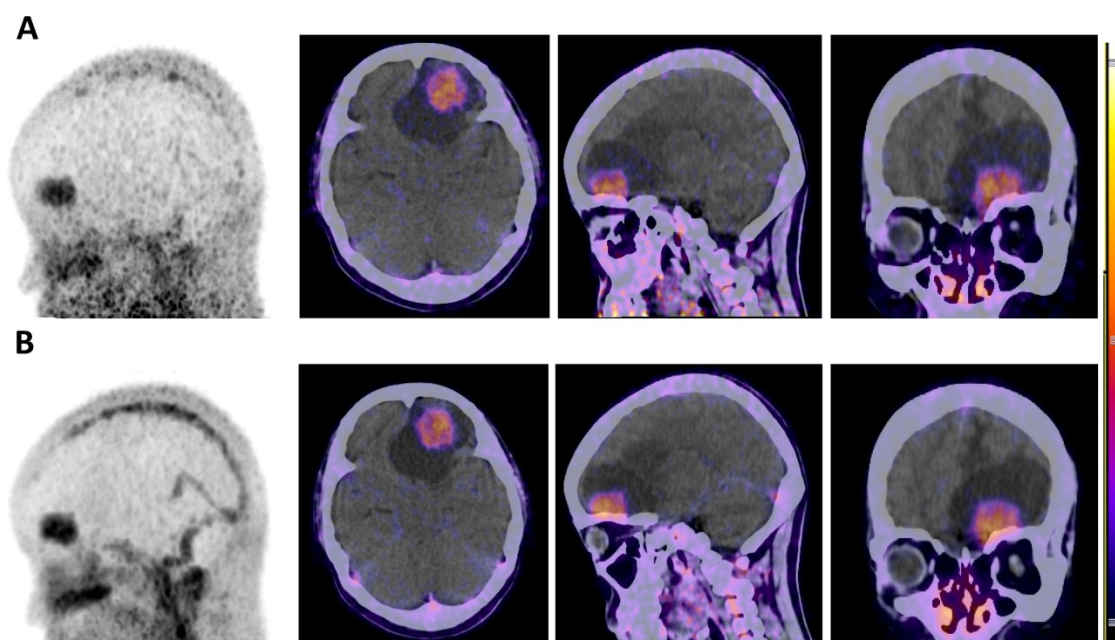
Fig. 3. Similar uptakes of the ^{68}Ga-NOTA-BBN and ^{68}Ga-IRDye800-NOTA-BBN tracers in PET/CT for a newly-diagnosed GBM patient. **(A)** ^{68}Ga-NOTA-BBN (7-14) PET MIP and PCT/CT images 30 min after ^{68}Ga-NOTA-BBN infusion. **(B)** ^{68}Ga-IRDye800-NOTA-BBN (7-14) PET MIP and PCT/CT images 60 min after ^{68}Ga-IRDye800-NOTA-BBN administration.

The intraoperative IRDye800CW-BBN FGS appeared to have clear advantages as illustrated by the example of Patient 3 displayed in Figure 4. When the dura was opened, the tumor fluorescence in the cortical area was obvious and was not affected by the superficial blood due to enough washout interval (**Fig. 4B**). After surgery, the residual tumor could not be differentiated from the adjacent brain tissue by white light microscopy but clearly showed positive fluorescence in the deep tumor cavity by the dual-modality imaging (**Fig. 4C**). After all fluorescent areas were totally resected (**Fig. 4D**), the postoperative MRI did not show residual enhancement (**Fig. 4E**). The pathology and GRPR immunostaining analysis confirmed the accuracy of fluorescence-based sampling and GRPR specificity (**Fig. 4G-J**).

With the strictest criteria of less than 0.175 cm^3 as complete resection [5], 7 patients achieved complete resection. For newly diagnosed GBM, complete resection was achieved in 6 out of 8 patients except for Patients 4 and 5, who had deep-seated tumors located in the thalamus and medial temporal insula, respectively eloquence grade III and grade II. In recurrent GBM, complete resection was achieved in 1 out of 6 patients due to the extremely huge area of contrast enhancement and radionecrosis following surgical intervention, radiotherapy, and chemotherapy. However, if we considered complete resection as removal of more than 95% of the initially enhanced tumor volume [8], the probe helped achieve complete resection in 9 patients, especially 7 among 8 newly diagnosed GBM patients.

We compared the intraoperative fluorescence signals with the residual enhancement areas in postoperative MRIs (**Table 1**). If the visible fluorescence was left in tumor cavity to protect the involved eloquent areas, the postoperative MRI showed residual contrast-enhanced tumors in the same position except in Patient 1 with complete resection of tumor but minimal fluorescence in the deep tumor cavity. Examples of details of contrast enhanced MRI, both from the residual tumors in postoperative MRI and intraoperative fluorescence left in the cavity, are shown in **Fig. S1** for Patient 4, **Fig. S2** for Patient 5, **Fig. S3** for Patient 9, **Fig. S4** for Patient 11, **Fig. S5** for Patient 12, and **Fig. S6** for Patient 14. These figures showed that the intraoperative fluorescence was identical to the enhancement in the postoperative MRI, which were eloquent areas that had to be protected intraoperatively.

In vivo and *ex vivo* fluorescence and correlation with pathology

The optical probe was uptaken well by the tumor and washed out by the adjacent normal brain. The RFU of the tumors were significantly higher than those in the background *in vivo* (137.9 ± 67.3 *vs.* 41.6 ± 24.2, p < 0.0001) and *ex vivo* (142.2 ± 38.3 *vs.* 33.0 ± 12.7, p < 0.0001). The SBR of the *in vivo* and *ex vivo* tissue was not significantly different (**Fig. 5**).
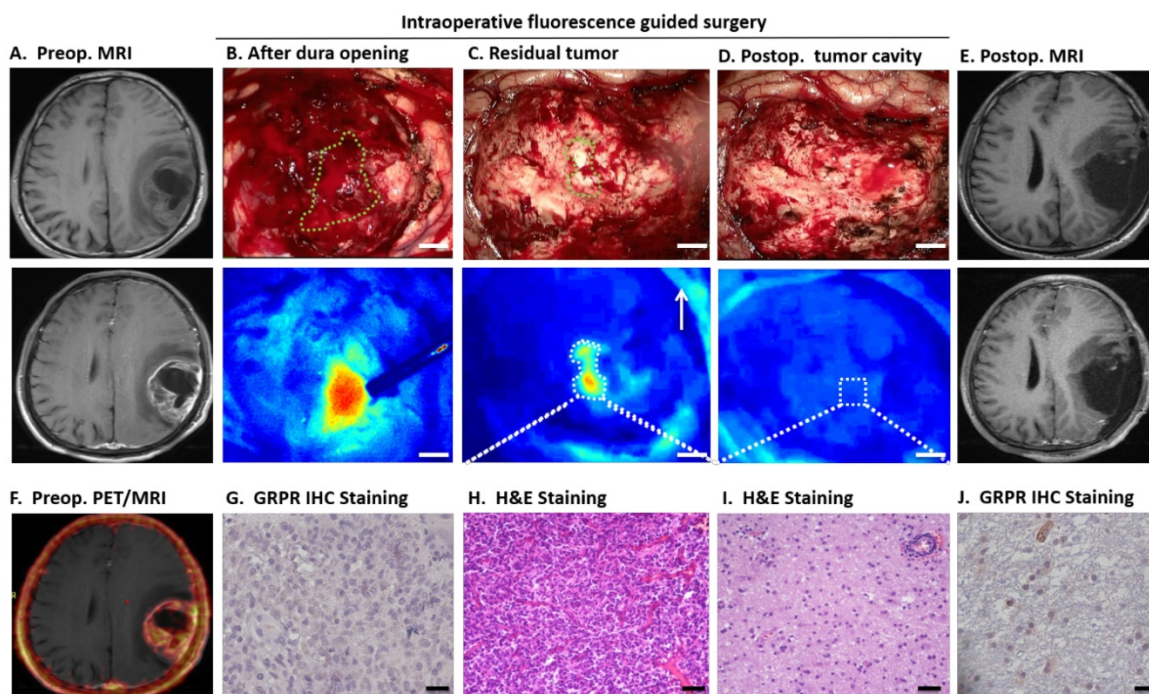
Fig. 4. ⁶⁸Ga-IRDye800-BBN PET/NIRF dual-modality imaging guided GBM resection for patient 3. Axial T$_1$-weighted (T1W) MRI showed a left temporal and parietal glioblastoma (eloquence III) in a 55-year-old man and obvious enhancement 30 min after intravenous injection of gadolinium (**A**). The fused ⁶⁸Ga-BBN PET/MRI showed positive probe uptake with clear margin (**F**). After dura opening, the fluorescent tumor was obviously seen by the NIRF imaging system, and indicated with the green dashed line in the white-light imaging (**B**, Scale bar, 5mm.). Of note, the blood was not fluorescent and did not influence the tumor visualization. It was difficult to differentiate the residual tumor (indicated with green dashed line) and adjacent normal brain tissue by intraoperative white-light microscope (**C**); however, the residual tumor was fluorescent in the deep tumor cavity (**C**) and was confirmed by H&E staining (**H**, scale bar 50um) and had abundant GRPR positive cells (**G**, scale bar 20um). After resecting the residual fluorescent tumor, the cavity showed no fluorescence (**D**) and further small tissue foci along the cavity was confirmed as normal brain tissue by H&E staining (**H**) and only a few scattered GRPR positive cells can be found (**J**). The postoperative enhancing MRI demonstrated complete resection of enhanced region (**E**).

A total of 31 fluorescent and 11 nonfluorescent *ex vivo* specimens were obtained intraoperatively. The details of their location, fluorescence signal, pathology, and WHO grading were shown in **Table S2**. Examples of two nonfluorescent tumor specimens from Patient 12 were displayed in **Fig. S7B and Fig. S7C**. These two specimens were false negatives, one of which was the tumor boundary tissue with scattered tumor cells in the brain tissue with a large amount of atypical gliosis; the other was diagnosed as oligodendroglioma and astrocytoma with an aggressive growth pattern in the low-grade region of the tumor. These examples indicate that relatively smaller density of tumor cells or lower grade areas of the secondary GBM might be nonfluorescent.

The match between the NIRF signal and pathology was summarized in **Table S3**. The sensitivity was calculated to be 93.9% (31/33, 95% CI 79.8%-99.3%). The specificity was very strict with normal brain tissue and no evidence of any grade of tumor and was 100% (9/9, 95% CI 66.4%-100%). Therefore, the specimen-by-specimen analysis yielded a diagnostic accuracy of 95.2% (40/42). With stringent pathology criteria for all grades of glioma, the positive predictive value (PPV) and the negative predictive value (NPV) were 100% (95% CI 88.8%-100%) and 81.8% (95% CI 48.2%-97.7%), respectively. To quantify the fluorescence signal, the SBR of pathology demonstrated GBM *ex vivo* tissue was significantly higher than that of non GBM (4.91 ± 0.61 *vs.* 1.14 ± 0.19, p = 0.0003).

Safety and adverse effects

Patients' discomforts and other safety issues (liver and renal toxicity and pyrogenic effect) of IRDye800CW-BBN tracer after intraoperative utilizeation are presented in **Table S1**. No allergy or renal function damage was noticed. Hepatic enzymes, especially glutamic-pyruvic transaminase, were initially increased in most patients within the first week after surgery but subsequently normalized with no clinical significance. Five patients had fever within 4 to 7 days postoperatively. The PCNSI or aseptic meningitis were confirmed by the clinical manifestation and cerebrospinal fluid analysis. Among the 14 patients enrolled, 11 patients complained of transient nausea which usually disappeared within 15 minutes.

Patient survival

As shown in **Table 2**, all patients were followed up with the median period of 6.5 months (range

1.5-18.9 months). The pathologic molecular profiling associated with patients' survival, including MGMT methylation status, TERT mutational status, IDH mutational status and 1p19q codeletion status, and postoperative therapy were also shown. Among the 5 newly diagnosed GBM patients with longer than 6 months follow-up, 4 patients achieved PFS-6, thus the PFS-6 was 80%. Of note, Patients 1 and 3 with complete resection and following treatment of standard Stupp protocol did not progress after 16.2 and 12.2 months since operation. Even for the recurrent GBM with complete resection in Patient 10, the tumor did not progress after 18.8 months.

Discussion

There is a critical need for a specific tumor visualization technique capable of distinguishing the tumor from normal brain intraoperatively that can assist surgeons to achieve gross total resection of the infiltrative GBM while benefiting patients by protecting neurological functions. In the past, a variety of anatomical imaging techniques have been utilized for guiding tumor resection, such as MRI-based neuronavigation, intraoperative ultrasound and MRI (iMRI), and metabolism-based intraoperative imaging, such as 5-ALA or fluorescein sodium-induced fluorescence imaging. These techniques improved gross total resection (from 69.1%-84.4%) and led to significant prolongation of PFS [5, 36-39]. However, there are limitations to each of these techniques. The navigation system cannot solve the intraoperative brain shift and is difficult to precisely resect the tissue based on the preoperative MRI navigation. In addition to being cost prohibitive, iMRI disrupts the flow of surgery adding at least one additional hour of operative time and cannot integrate with PET imaging intraoperatively. 5-ALA optical imaging has relatively low sensitivity and specificity particularly in heterogeneous tumors [14, 40, 41]. Furthermore, these techniques cannot evaluate the same specific tumor target pre- and intraoperatively.

In the present study, we developed a unique dual-modality PET/optical imaging probe which was based on our previously described ^{68}Ga-BBN PET tracer to specifically image the GRPR receptor expression *in vivo* on gliomas of different WHO grades [16]. This is the first translational study performed in GBM patients comparing the preoperative GRPR receptor biodistribution with the traditionnal gadolinium enhancement in MRI. This unique dual-modality imaging probe not only enabled preoperative assessment for resection accuracy but also allowed real-time optical navigation intraoperatively for achieving maximal safe resection.

We observed a strong correlation between the PET uptake, fluorescence, and GBM pathology, indicating that the tracer uptake was a result of specific GRPR binding. Several significant advantages of this probe in the first-in-human study were obvious. First, an extremely low dose of probe was sufficient for PET/optical imaging (40 µg per patient for preoperative PET and 1 mg per patient for intraoperative optical imaging
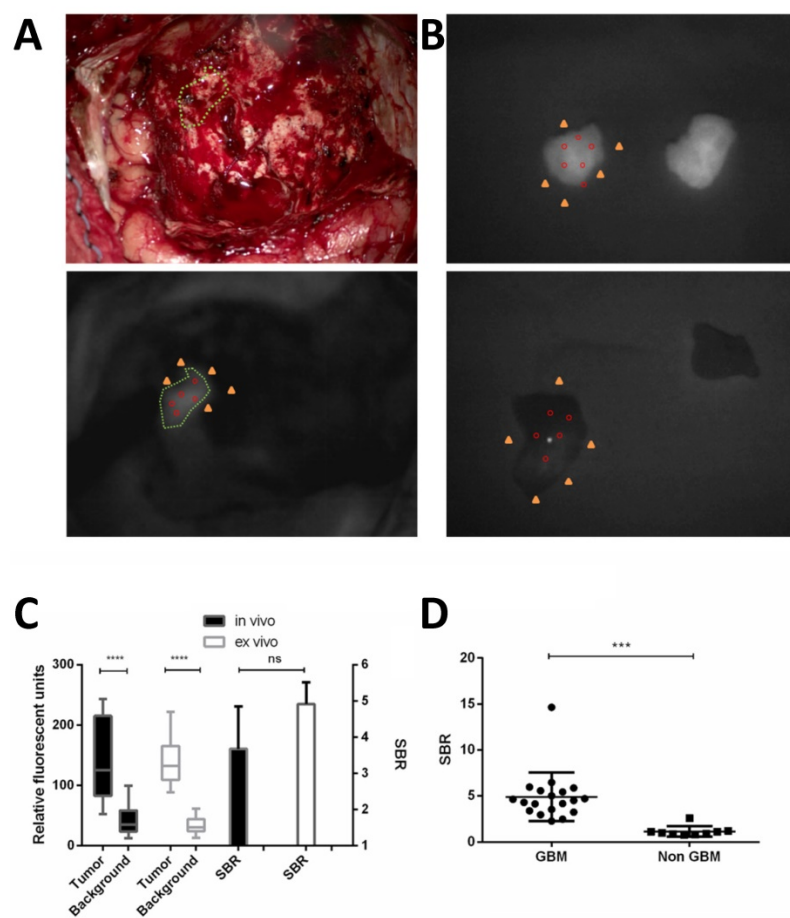
Fig. 5. Quantification of fluorescence imaging for *in vivo* and *ex vivo* pathology demonstrated GBM or adjacent brain tissue. Relative fluorescent units (RFU) were acquired during intraoperative fluorescent imaging of residual tumor *in vivo* and NIRF region superimposed on white light (**A**). The *ex vivo* tissue of the fluorescent GBM tissue and adjacent brain tissue both demonstrated by pathology were shown in (**B**). Example of RFU calculation is shown. Five points are chosen in the fluorescent gross tumor (red circles) and another five points in the surrounding cortical or tumor cavity as background (yellow triangles), the mean RFU are calculated and the Signal-to-background ratio (SBR) is thus calculated. The RFU of the tumor were significantly higher (****$p < 0.0001$) than those in the background, *in vivo* and *ex vivo*. But the SBR of *in vivo* and *ex vivo* tissue was not different significantly (**C**). The SBR of pathology demonstrated GBM *ex vivo* tissue was significantly higher (***$p < 0.001$) than that of non GBM. Data are RFU and SBR ± SD.

vs. 20 mg/kg for oral 5-ALA and 5 mg/kg for intravenous fluorescein sodium). Second, the dual-modality probe could be used preoperatively and intraoperatively and was both safe and well-tolerated. And third, compared to the white light microscope identifying tumors based on superficial texture or color change, this near-infrared fluorescence-based technique was far more sensitive. This was especially helpful in detecting the residual foci with penetration depths of up to several millimeters after debulking most of the tumor and ensuring tumor resection within the tumor range and not damaging the adjacent normal brain. This cohort achieved 80% PFS-6 for newly-diagnosed GBM patients, higher than 46% in those of 5-ALA [42]. The PFS of the two patients with complete resection, more than 16.2 and 12.2 months, were longer than reported before (median PFS, 7 months [13] and 6.9 months [43]). Thus, this dual-modality imaging GRPR-specific probe could be utilized intraoperatively to visualize tumor margins without brain shift and might improve patient survival.

The trial of 5-ALA and fluorescein only enrolled newly diagnosed, untreated malignant glioma patients and excluded patients with tumors of the midline, basal ganglia, and other locations that did not allow complete resection [5, 13]. Our series of 14 GBM patients included 8 newly diagnosed and 6 recurrent GBM, among which 10 patients having tumors of eloquence grade III and 2 with eloquence grade II. In order to protect the neurofunctions, the tumors in some patients were not able to be resected completely. Another operation influencing factor was the preoperative tumor volume. The median volume based on enhancing T1 weighted MRI in this cohort was 55.49 cm^3, which was much larger than that in a phase II study of fluorescein-guided surgery (28.75 cm^3) [13]. Significantly, of the 8 newly diagnosed GBM, 6 patients achieved complete resection even with 5 tumors in eloquent brain areas as eloquence grade III. In the other 2 patients, complete resection was not possible as one tumor was in the thalamus involving midbrain and the other was in the temporal and insula lobe. Although the residual tumors exhibited positive fluorescence in resection cavity intraoperatively, complete resection was avoided to protect neurofunctions.

Table 2. Patient follow-up data including postoperative therapy, the survival profile and associated pathology profiling.

Patient No.	Molecular pathology profiling	Complete resection (Y/N)	Follow-up duration (months)	Postoperative therapy	PFS for newly GBM (months)	OS for newly GBM (months)	OS for recurrent GBM (months)
1	MGMT(+),1p19q codeletion(-)	Y	16.2	RT + concomitant TMZ + TMZ (6)	16.2+	/	/
2	MGMT(+),TERTmutation(+), IDHmutation(-), 1p19q codeletion(-)	Y	9.2	TMZ (5)	3.9	9.2	/
3	MGMT(+),TERTmutation(-), IDHmutation(+), 1p19q codeletion(-)	Y	12.2	RT + concomitant TMZ + TMZ (10)	12.2+	/	/
4	MGMT(-),TERTmutation(-), IDHmutation(-), 1p19q codeletion(-)	N	8.1	TMZ (6)	7.4	8.1	/
5	MGMT(+),TERTmutation(+), IDHmutation(+), 1p19q codeletion(-)	N	6.4	RT + concomitant TMZ +TMZ (6)	6.4+	/	/
6	MGMT(-),TERTmutation(-), IDHmutation(-), 1p19q codeletion(+)	Y	2.0	RT + PCV chemotherapy	2.0+	/	/
7	MGMT(+),TERTmutation(+), IDHmutation(-)	Y	1.5	RT + concomitant TMZ	1.5+	/	/
8	MGMT(+),TERTmutation(+), IDHmutation(-)	Y	1.5	RT + concomitant TMZ	1.5+	/	/
9	MGMT(-),IDHmutation(-), 1p19q codeletion(-)	N	6.4	No	/	/	6.4
10	MGMT(-),IDHmutation(-), 1p19q codeletion(-)	Y	18.9	No	/	/	18.9+
11	MGMT(+),IDHmutation(+), 1p19q codeletion(-)	N	1.5	No	/	/	1.5
12	MGMT(+),IDHmutation(+), 1p19q codeletion(-)	N	6.5	TMZ (5)	/	/	6.5
13	MGMT(-),TERTmutation(+), IDHmutation(+), 1p19q codeletion(-)	N	10.6	TMZ + bevacizumab (5)	/	/	10.6
14	MGMT(+),TERTmutation(+), IDHmutation(-), 1p19q codeletion(-)	N	5.5	RT + concomitant TMZ + TMZ (6)	/	/	5.5

RT (radiotherapy), TMZ (temozolomide), PCV (procarbazine, lomustine, vincristine), PFS (Progression-free survival), OS (Overall survival).

At this point, the optical imaging technique was not optimal for the deep-seated tumors (Patients 4 and 5) and, due to the light diffusion in deep tumor cavity, the SBR was not adequate during surgery. In future clinical trials, the correlation between the NIRF intensity and cellularity, proliferation index, and other molecular pathological characteristics will be analyzed to further optimize the dual-imaging probe. Although the technique appears to have significant potential for larger safe extent of resection and better prognosis, the limited number of patients with insufficient follow-up interval did not allow more definitive correlation of this technique with clinical outcomes. Future work will be designed in randomized clinical trials with more strict inclusion criteria, for example enrollment of only newly diagnosed patients with GBM eligible for total resection, to assess the effectiveness of this technique in improving patient survival.

In conclusion, this first-in-human study highlights an approach that uses the PET/NIRF dual-modality technique with ^{68}Ga-IRDye800CW-BBN in the preoperative assessment and FGS of GBM. This novel imaging probe has demonstrated its potential for maximum safe resection of difficult to access tumors without damaging the normal brain tissue.

Acknowledgements

Author contributions

The project was initially conceptualized and the entire project was supervised by D.L., J.Z., Z.Z. and X.C. The preclinical study and NIRF navigation system were supervised by J.T. Clinical trial leads were Z.Z., L.Z. and N.J. and the operation were done by N.J. Image/data acquisition was performed by J.Z., D.L., C.C., X.X. and N.J. All authors participated in the interpretation of the reported experiments or results. D.L., J.Z. C.C. and I.A. wrote the manuscript, which was then further refined by Z.Z., N.J. and X.C. All other authors reviewed the final version of the manuscript.

Supplementary Material

Supplementary figures and tables.
http://www.thno.org/v08p2508s1.pdf

Competing Interests

The authors have declared that no competing interest exists.

References

1. Marko NF, Weil RJ, Schroeder JL, Lang FF, Suki D, Sawaya RE. Extent of resection of glioblastoma revisited: personalized survival modeling facilitates more accurate survival prediction and supports a maximum-safe-resection approach to surgery. J Clin Oncol. 2014; 32: 774-82.
2. Suchorska B, Weller M, Tabatabai G, Senft C, Hau P, Sabel MC, et al. Complete resection of contrast-enhancing tumor volume is associated with improved survival in recurrent glioblastoma-results from the DIRECTOR trial. Neuro Oncol. 2016; 18: 549-56.
3. Shah AH, Snelling B, Bregy A, Patel PR, Tememe D, Bhatia R, et al. Discriminating radiation necrosis from tumor progression in gliomas: a systematic review what is the best imaging modality? J Neurooncol. 2013; 112: 141-52.
4. Suchorska B, Jansen NL, Linn J, Kretzschmar H, Janssen H, Eigenbrod S, et al. Biological tumor volume in 18FET-PET before radiochemotherapy correlates with survival in GBM. Neurology. 2015; 84: 710-9.
5. Stummer W, Pichlmeier U, Meinel T, Wiestler OD, Zanella F, Reulen HJ. Fluorescence-guided surgery with 5-aminolevulinic acid for resection of malignant glioma: a randomised controlled multicentre phase III trial. Lancet Oncol. 2006; 7: 392-401.
6. Hingtgen S, Figueiredo JL, Farrar C, Duebgen M, Martinez-Quintanilla J, Bhere D, et al. Real-time multi-modality imaging of glioblastoma tumor resection and recurrence. J Neurooncol. 2013; 111: 153-61.
7. Hadjipanayis CG, Widhalm G, Stummer W. What is the Surgical Benefit of Utilizing 5-Aminolevulinic Acid for Fluorescence-Guided Surgery of Malignant Gliomas? Neurosurgery. 2015; 77: 663-73.
8. Teixidor P, Arraez MA, Villalba G, Garcia R, Tardaguila M, Gonzalez JJ, et al. Safety and Efficacy of 5-Aminolevulinic Acid for High Grade Glioma in Usual Clinical Practice: A Prospective Cohort Study. PLoS One. 2016; 11: e0149244.
9. Schebesch KM, Proescholdt M, Hohne J, Hohenberger C, Hansen E, Riemenschneider MJ, et al. Sodium fluorescein-guided resection under the YELLOW 560 nm surgical microscope filter in malignant brain tumor surgery--a feasibility study. Acta Neurochir (Wien). 2013; 155: 693-9.
10. Acerbi F, Cavallo C, Broggi M, Cordella R, Anghileri E, Eoli M, et al. Fluorescein-guided surgery for malignant gliomas: a review. Neurosurg Rev. 2014; 37: 547-57.
11. Rey-Dios R, Hattab EM, Cohen-Gadol AA. Use of intraoperative fluorescein sodium fluorescence to improve the accuracy of tissue diagnosis during stereotactic needle biopsy of high-grade gliomas. Acta Neurochir (Wien). 2014; 156: 1071-5; discussion 5.
12. Zhao S, Wu J, Wang C, Liu H, Dong X, Shi C, et al. Intraoperative fluorescence-guided resection of high-grade malignant gliomas using 5-aminolevulinic acid-induced porphyrins: a systematic review and meta-analysis of prospective studies. PLoS One. 2013; 8: e63682.
13. Acerbi F, Broggi M, Schebesch KM, Hohne J, Cavallo C, De Laurentis C, et al. Fluorescein-Guided Surgery for Resection of High-Grade Gliomas: A Multicentric Prospective Phase II Study (FLUOGLIO). Clin Cancer Res. 2018; 24: 52-61.
14. Jaber M, Wolfer J, Ewelt C, Holling M, Hasselblatt M, Niederstadt T, et al. The Value of 5-Aminolevulinic Acid in Low-grade Gliomas and High-grade Gliomas Lacking Glioblastoma Imaging Features: An Analysis Based on Fluorescence, Magnetic Resonance Imaging, 18F-Fluoroethyl Tyrosine Positron Emission Tomography, and Tumor Molecular Factors. Neurosurgery. 2016; 78: 401-11; discussion 11.
15. Flores DG, Meurer L, Uberti AF, Macedo BR, Lenz G, Brunetto AL, et al. Gastrin-releasing peptide receptor content in human glioma and normal brain. Brain Res Bull. 2010; 82: 95-8.
16. Zhang J, Li D, Lang L, Zhu Z, Wang L, Wu P, et al. 68Ga-NOTA-Aca-BBN (7-14) PET/CT in Healthy Volunteers and Glioma Patients. J Nucl Med. 2016; 57: 9-14.
17. Cohen R, Vugts DJ, Stigter-van Walsum M, Visser GW, van Dongen GA. Inert coupling of IRDye800CW and zirconium-89 to monoclonal antibodies for single- or dual-mode fluorescence and PET imaging. Nat Protoc. 2013; 8: 1010-8.
18. Rosenthal EL, Warram JM, de Boer E, Chung TK, Korb ML, Brandwein-Gensler M, et al. Safety and Tumor Specificity of Cetuximab-IRDye800 for Surgical Navigation in Head and Neck Cancer. Clin Cancer Res. 2015; 21: 3658-66.
19. Zinn KR, Korb M, Samuel S, Warram JM, Dion D, Killingsworth C, et al. IND-directed safety and biodistribution study of intravenously injected cetuximab-IRDye800 in cynomolgus macaques. Molecular imaging and

biology : MIB : the official publication of the Academy of Mol Imaging. 2015; 17: 49-57.

20. Center D-HM. A Microdose Evaluation Study of ABY-029 in Recurrent Glioma (ABY-029). https://clinicaltrialsgov/ct2/show/NCT02901925.

21. Rosenthal E. Phase I Panitumumab IRDye800 Optical Imaging Study. https://clinicaltrialsgov/ct2/show/NCT02415881.

22. van Dam GM. VEGF-targeted Fluorescent Tracer Imaging in Breast Cancer. http://clinicaltrialsgov/show/NCT01508572.

23. Lamberts LE, Koch M, de Jong JS, Adams ALL, Glatz J, Kranendonk MEG, et al. Tumor-Specific Uptake of Fluorescent Bevacizumab-IRDye800CW Microdosing in Patients with Primary Breast Cancer: A Phase I Feasibility Study. Clin Cancer Res. 2017; 23: 2730-41.

24. Rosenthal EL, Moore LS, Tipirneni K, de Boer E, Stevens TM, Hartman YE, et al. Sensitivity and Specificity of Cetuximab-IRDye800CW to Identify Regional Metastatic Disease in Head and Neck Cancer. Clin Cancer Res. 2017; 23: 4744-52.

25. Liu Z, Niu G, Wang F, Chen X. (68)Ga-labeled NOTA-RGD-BBN peptide for dual integrin and GRPR-targeted tumor imaging. Eur J Nucl Med Mol Imaging. 2009; 36: 1483-94.

26. Wen PY, Macdonald DR, Reardon DA, Cloughesy TF, Sorensen AG, Galanis E, et al. Updated response assessment criteria for high-grade gliomas: response assessment in neuro-oncology working group. J Clin Oncol. 2010; 28: 1963-72.

27. Chi C, Du Y, Ye J, Kou D, Qiu J, Wang J, et al. Intraoperative imaging-guided cancer surgery: from current fluorescence molecular imaging methods to future multi-modality imaging technology. Theranostics. 2014; 4: 1072-84.

28. Mao Y, Wang K, He K, Ye J, Yang F, Zhou J, et al. Development and application of the near-infrared and white-light thoracoscope system for minimally invasive lung cancer surgery. J Biomed Opt. 2017; 22: 66002.

29. He K, Chi C, Kou D, Huang W, Wu J, Wang Y, et al. Comparison between the indocyanine green fluorescence and blue dye methods for sentinel lymph node biopsy using novel fluorescence image-guided resection equipment in different types of hospitals. Transl Res. 2016; 178: 74-80.

30. Chi C, Zhang Q, Mao Y, Kou D, Qiu J, Ye J, et al. Increased precision of orthotopic and metastatic breast cancer surgery guided by matrix metalloproteinase-activatable near-infrared fluorescence probes. Sci Rep. 2015; 5: 14197.

31. Lee JYK, Cho SS, Zeh R, Pierce JT, Martinez-Lage M, Adappa ND, et al. Folate receptor overexpression can be visualized in real time during pituitary adenoma endoscopic transsphenoidal surgery with near-infrared imaging. J Neurosurg. 2017: 1-14.

32. Sorensen AG, Patel S, Harmath C, Bridges S, Synnott J, Sievers A, et al. Comparison of diameter and perimeter methods for tumor volume calculation. J Clin Oncol. 2001; 19: 551-7.

33. Louis DN, Perry A, Reifenberger G, von Deimling A, Figarella-Branger D, Cavenee WK, et al. The 2016 World Health Organization Classification of Tumors of the Central Nervous System: a summary. Acta Neuropathol. 2016; 131: 803-20.

34. Bossuyt PM, Reitsma JB, Bruns DE, Gatsonis CA, Glasziou PP, Irwig L, et al. STARD 2015: an updated list of essential items for reporting diagnostic accuracy studies. BMJ. 2015; 351: h5527.

35. Sawaya R, Hammoud M, Schoppa D, Hess KR, Wu SZ, Shi WM, et al. Neurosurgical outcomes in a modern series of 400 craniotomies for treatment of parenchymal tumors. Neurosurgery. 1998; 42: 1044-55; discussion 55-6.

36. Mahboob S, McPhillips R, Qiu Z, Jiang Y, Meggs C, Schiavone G, et al. Intraoperative Ultrasound-Guided Resection of Gliomas: A Meta-Analysis and Review of the Literature. World Neurosurg. 2016; 92: 255-63.

37. Gessler F, Forster MT, Duetzmann S, Mittelbronn M, Hattingen E, Franz K, et al. Combination of Intraoperative Magnetic Resonance Imaging and Intraoperative Fluorescence to Enhance the Resection of Contrast Enhancing Gliomas. Neurosurgery. 2015; 77: 16-22; discussion

38. Kuhnt D, Becker A, Ganslandt O, Bauer M, Buchfelder M, Nimsky C. Correlation of the extent of tumor volume resection and patient survival in surgery of glioblastoma multiforme with high-field intraoperative MRI guidance. Neuro Oncol. 2011; 13: 1339-48.

39. Senft C, Bink A, Franz K, Vatter H, Gasser T, Seifert V. Intraoperative MRI guidance and extent of resection in glioma surgery: a randomised, controlled trial. Lancet Oncol. 2011; 12: 997-1003.

40. Hauser SB, Kockro RA, Actor B, Sarnthein J, Bernays RL. Combining 5-Aminolevulinic Acid Fluorescence and Intraoperative Magnetic Resonance Imaging in Glioblastoma Surgery: A Histology-Based Evaluation. Neurosurgery. 2016; 78: 475-83.

41. Widhalm G, Wolfsberger S, Minchev G, Woehrer A, Krssak M, Czech T, et al. 5-Aminolevulinic acid is a promising marker for detection of anaplastic foci in diffusely infiltrating gliomas with nonsignificant contrast enhancement. Cancer. 2010; 116: 1545-52.

42. Stummer W, Tonn JC, Mehdorn HM, Nestler U, Franz K, Goetz C, et al. Counterbalancing risks and gains from extended resections in malignant glioma surgery: a supplemental analysis from the randomized 5-aminolevulinic acid glioma resection study. Clinical article. J Neurosurg. 2011; 114: 613-23.

43. Stupp R, Mason WP, van den Bent MJ, Weller M, Fisher B, Taphoorn MJ, et al. Radiotherapy plus concomitant and adjuvant temozolomide for glioblastoma. N Engl J Med. 2005; 352: 987-96.